A New Protection Scheme for Feeders of Microgrids with Inverter-Based Resources

Jigyesh Sharma, *Senior Member IEEE* Tarlochan S Sidhu, *Fellow IEEE*

***Abstract*-- Due to the unavailability of a suitable relay for microgrid protection, various utilities are fitting available IEDs for the protection of microgrids. At present, microgrid protection is achieved using a combination of conventional numerical relays. These numerical relays are not suitable for all kinds of microgrid architectures and do not provide complete protection with inverter-based generators. Since these relays were designed considering the fault characteristics of synchronous generators, they fail to respond to the fault characterized by inverter-based generators. This paper proposes a new protection technique that is independent of the type of generating sources, control philosophy of inverters as well as microgrid architecture. Simulations are performed using PSCAD/EMTDC and performance of the protection scheme is also evaluated in real-time using RTDS. Pertinent results are presented which demonstrate the effectiveness of the proposed scheme.**

***Keywords*—Microgrid protection, distributed energy resources, digital relays, phasor measurement unit**

I. Introduction

Microgrids are a part of present and future electrical power system networks. The expansion of the network with decentralized generation using renewable sources of energy with inverter-based resources is increasing rapidly. Renewable energy sources are not only used as backup generators but also provide a wide range of benefits when formed as part of microgrids. Microgrids provide several environmental and economic benefits to utilities as well as to consumers [1]. Inverter-based distributed generators are broadly classified into grid-forming and grid-following inverters. Grid-following inverters are grid connected inverters that track the frequency and phase of the voltage waveform of the grid and the output current is synchronized with the grid, hence it is fundamentally a current source system. The types of commonly used grid following inverters are PV, wind, etc. While grid-forming inverters generate their own reference which is constantly adjusted according to the output power of the inverter [2]. The most commonly used grid-forming inverters are battery storage energy system. In Reference [3], grid following inverter is defined as an inverter to export the set power into the grid and the grid-forming inverter is to regulate voltage and frequency.

The protection of microgrids with inverter-based distributed generators possess several challenges owing to their varied operation and control philosophies.

J. Sharma is a graduate research student in the Department of Electrical and Computer Engineering at Ontario Tech University, Canada (e-mail:jigyesh.sharma@ontariotechu.net).

T.S. Sidhu is a professor in the Department of Electrical and Computer Engineering at Ontario Tech University, Canada (e-mail of corresponding author: Tarlochan.sidhu@ontariotechu.ca).

Paper submitted to the International Conference on Power Systems Transients (IPST2023) in Thessaloniki, Greece, June 12-15, 2023.

Some of the challenges to microgrid protection are due to limited fault current and dynamic of fault current due to changes in topology, bi-directional flow of fault current, variations in short circuit level due to different operating modes such as islanded mode and grid-connected mode, sympathetic tripping, loss of coordination [4]-[7]. Various practices followed for the protection of microgrids in North America are described in [8] and there is no single relay available commercially which fits all types of microgrid architecture.

Before applying a protection strategy for a microgrid, it is important to understand its fault characteristics under different operating scenarios. In [9], protection of the microgrid is performed using inverse time characteristics of IEC 60255, the inverse time characteristics based protection strategy is suitable when the magnitude of the fault current is larger than the full load current of the feeder, otherwise, the time operation of relay for fault current provided by the inverter which is 1 to 2 p.u [10]-[12], won't provide quick isolation during a fault and coordination amongst the relays would be a challenge. In [13], negative sequence current and zero sequence current based protection strategies are proposed but, in many inverters, due to filter modules, only positive sequence components are delivered to the control system and, negative and zero sequence currents are suppressed to zero [14] except when zero-sequence currents can be supplied from grid through transformer neutral. In [15]-[18], principle of differential current is used for the protection of feeders, since fault current itself is limited when the microgrid is operating with all inverter-based resources in grid-isolated mode, the difference of current after accounting for CT errors and relay errors may not be sufficient for the relay to pick up. In [19][20], adaptive relaying is used for the protection of microgrids. This strategy determines the setting based on changes in the operating scenario by performing fault analysis and uses inverse time characteristics with the directional feature. Such a strategy is complex with meshed networks and in real-time, as too many complex analyses need to be performed. Also, the fault current signature changes when the inverter switches between operating modes e.g. P-Q to V-F [21]. In [22], protection strategy using the undervoltage function is proposed but during islanded mode, the voltage in the network is severely affected by the type of fault and location of the fault. Further, in islanded mode, the inverter regulates the voltage to meet the requirements of LVRT [23], hence voltage-based protection alone is not adequate for microgrid protection. The fault response of an inverter is governed by its adopted control strategy and the control strategy changes as per the network requirements [24]. The phase angle relationship between the voltage and current of inverter-based resources is variable and cannot be predicted [25], therefore, protection based on directional overcurrent and its sequence components using commercially available relays may not be adequate. The low magnitude of fault current in microgrids is a well-known

phenomenon when microgrids are operating with inverter-based resources. The conventional relay which uses a torque equation to establish the direction of current fails to generate enough torque in an islanded mode of microgrid operation [26]. Presently, microgrids are protected with commercially available relays since they are the only option available to utilities and power system operators. Some researchers have proposed non-traditional techniques [27] including adaptive methods; however, these techniques still suffer from limitations such as requiring up-to-date topology information or are only applicable for special situations. For example, the technique proposed in [28] is a directional comparison technique and is like a traditional directional comparison method. It may not perform well in high impedance faults and during change of angle due to control strategy of inverters. Also, the technique requires detection of fault before determining its location. This adds another uncertainty as fault detection in cases where fault current is low may not happen reliably. This paper develops a new relaying technique that is independent of control strategy, type of inverter, the capacity of the inverter and architecture of the microgrid. Protection philosophy and relay characteristics are described in Section II. Section III covers test results on a benchmark microgrid, and Section IV includes real time implementation results validated on RTDS™. Sections V and VI discuss the comparison with a differential relay and practical implementation of the proposed scheme respectively and Section VII concludes the paper.

II. Proposed Protection Philosophy and Relay Characteristics

The main inputs to a protection relay are voltage and current and other electrical parameters are derived from these values. The proposed scheme develops a new fault detection philosophy by estimating the positive sequence 'discrepant impedance' of the feeder. The voltage and current samples are obtained from two ends of the feeder. From these sampled values, positive sequence 'discrepant impedance' is calculated by the relay. The detailed theory and basis are described in the following sections.

A. No fault condition

To explain the calculation of discrepant impedance, a two bus microgrid with both ends connected with inverter-interfaced distributed generators is shown in Fig. 1. For a shunt fault at f at a distance x from Bus A , let the positive sequence voltages and currents at Bus-A and Bus-B be $V_{A1,}$ $I_{A1,}$ V_{B1}, and I_{B1} respectively. Z_1 is the positive-sequence impedance of the feeder between Bus-A and Bus-B. The voltage V_{B1} at Bus-B when current I_{A1} is flowing from Bus-A to Bus-B is: Fig. 1. Sequence

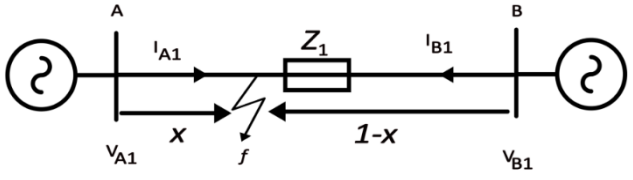

Fig. 1. Feeder connected at two ends by an inverter-based generator

$$\vec{V}_{B1} = \vec{V}_{A1} - \vec{I}_{A1}\ \overrightarrow{Z_1} \quad (1)$$

Then,

$$\overrightarrow{Z_1} = \frac{\vec{V}_{A1} - \vec{V}_{B1}}{\vec{I}_{A1}} \quad (2)$$

Z_1 is the positive-sequence impedance of the feeder as estimated from Bus-A using positive-sequence voltages from Bus-A and Bus-B, and positive-sequence current measured at Bus-A.

Similarly, the voltage at Bus-A will be,

$$\vec{V}_{A1} = \vec{V}_{B1} - \left(-\overrightarrow{I_{B1}}\ \overrightarrow{Z_1}\right) \quad (3)$$

Then,

$$-\overrightarrow{Z_1} = \frac{\overrightarrow{V_{B1}} - \overrightarrow{V_{A1}}}{\overrightarrow{I_{B1}}} \quad (4)$$

$-Z_1$ is the positive-sequence impedance of the feeder as estimated form Bus-B using positive-sequence voltages from Bus-A and Bus-B, and positive-sequence current measured at Bus-B.

Under no fault condition, I_{A1} is equal to $I_{B1.}$ Therefore, during no fault condition it can be observed from (2) and (4), the summation of the impedances $\overrightarrow{Z_1}$ and $-\overrightarrow{Z_1}$ is zero. This summation of impedances is termed as 'discrepant impedance'. This impedance signifies the discrepancy between the feeder impedances when estimated from one end of the line and the other end of the line.

B. Fault condition

Assume a fault occurs at distance *x* from the Bus-A in Fig. 1. The sequence impedance diagram for the faulted network is shown in Fig. 2.

Applying KVL in loop-1 and2, we get.

$$\overrightarrow{V_{A1}} = \overrightarrow{V_{f1}} + \overrightarrow{I_{A1}}\ \overrightarrow{xZ_1} \quad (5)$$

$$\overrightarrow{V_{B1}} = \overrightarrow{V_{f1}} + (-I_{B1})(1-x)\overrightarrow{Z_1} \quad (6)$$

Simplifying Equations (5) and (6),

$$\frac{\overrightarrow{V_{A1}} - \overrightarrow{V_{B1}}}{\overrightarrow{I_{A1}}} = \frac{\overrightarrow{I_{B1}}}{\overrightarrow{I_{A1}}}\overrightarrow{Z_1} - \frac{\overrightarrow{I_{B1}}}{\overrightarrow{I_{A1}}}\overrightarrow{Z_1}x + \overrightarrow{Z_1}x \quad (7)$$

$$\frac{\overrightarrow{V_{B1}} - \overrightarrow{V_{A1}}}{\overrightarrow{I_{B1}}} = -\overrightarrow{Z_1} + \overrightarrow{Z_1}x - \frac{\overrightarrow{I_{A1}}}{\overrightarrow{I_{B1}}}\overrightarrow{Z_1}x \quad (8)$$

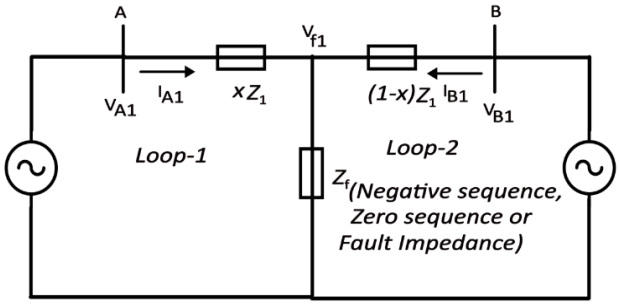

Fig. 2. Sequence impedance diagram for a shunt fault at f.

Where, V_{f1} is positive sequence component of fault voltage at the fault point f and Z_f is a combination of negative sequence, zero sequence or fault impedance depending upon the type of fault. Equations (7) and (8) represent positive sequence impedance of the feeder when estimated from Bus-A and Bus-B respectively. It is clear that the discrepant impedance during a fault will not be zero as is the case during a no-fault condition. Its exact value will depend on the fault location, currents and voltages during the fault.

C. *Discrepant impedance characterstics on R-X plane*

The R-X plot for the discrepant impedance estimated by the relay is shown in Fig. 3. Under no-fault condition, the circle shown is Fig. 3 shall theoretically have zero radius and lie at the origin. However, when the errors encountered during measurement of currents and voltages are accounted, therefore, the circle of no-fault region will have a small radius. For the studies reported in this paper, the radius of the no-fault region circle was selected to be 3% of the feeder impedance. In field applications, a setting close to 3-5% should suffice depending on the measurement accuracy of instrument transformers and required sensitivity of the relay. The relay will issue a trip command to the breaker after five consecutive values of discrepant impedances are in fault region as depicted in Fig. 3 trip logic.

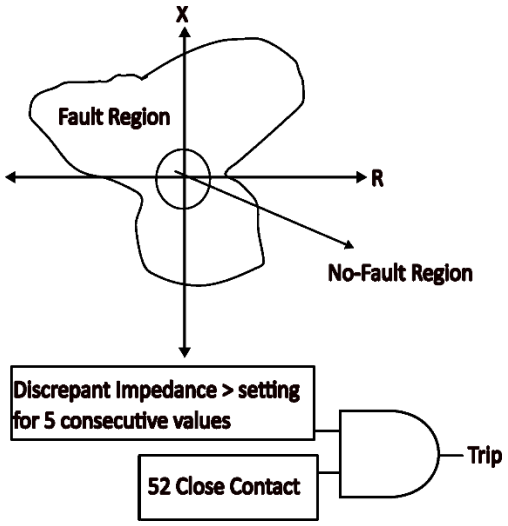

Fig. 3. Relay trip characteristics and trip logic.

III. TEST RESULTS

The IEEE-9 bus test system with the combination of grid forming and grid following inverters is developed in PSCAD. The model developed in reference [8] with modifications is used as a test bed for this paper. Load data, generation data and line parameters are provided in Table-I and Table-II of Appendix. Fig. 4 describes the network architecture of microgrid with three inverters, feeders and loads. Two inverters are operating as grid-forming inverters and one inverter is operating as grid-following inverter. Each inverter is rated at 200 MVA. Solar and wind resources were achieved using grid-following inverters whereas a battery source is connected via grid forming inverter. Loads connected at buses are constant impedance loads. The lines are modeled using a pi model. Positive-sequence voltages and currents are estimated at both ends of the line and discrepant impedances are estimated as discussed in Section II. The proposed protection philosophy is validated for different cases including different types of faults, fault locations, and type of inverter present in the network both in gird-connected and islanded modes.

A. *Islanded Mode of Operation*

In this operation mode, only inverter-based resources are connected to bus-1, 2 and 3 and grid is out of service. The inverters at bus-1 and bus-2 are grid forming and at bus-3 is grid following. The response of the proposed protection scheme for various types of faults at different locations is described in the following subsections.

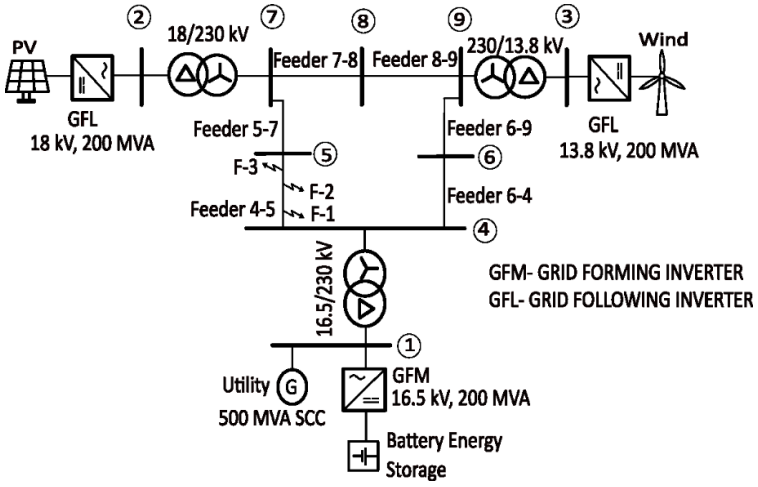

Fig. 4. IEEE 9 bus test microgrid.

1) *Different types of faults at different locations*

A single-phase fault, F-1, is simulated at 30 % of line length of feeder 4-5 from bus 4. The voltages at various buses during the fault F-1 are shown in Fig. 5. Before the fault, the voltages at the buses are close to 1 p.u. The discrepant impedances before the fault and during the fault are shown in Fig. 6. It is observed that the discrepant impedances estimated from two ends of line are in the no-fault region before the fault. Theoretically, discrepant impedances should be zero. The feeders are modelled using pi model, but the protection technique considers the feeder impedances as lumped values neglecting capacitances. Because of this difference, it is not exactly zero during no-fault condition.

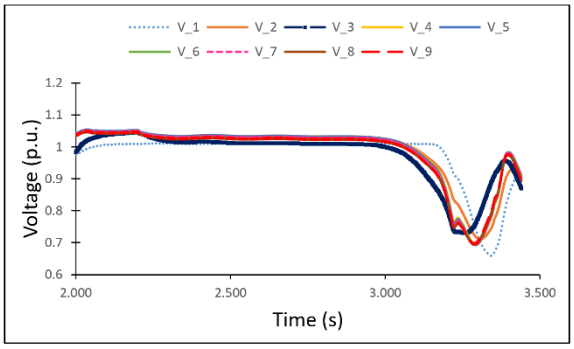

Fig. 5. Magnitude of voltages during a fault at F-1.

During the fault, discrepant impedances are in the fault region which can be observed in Fig. 6. The radius of the circle in Fig. 6 is not large, this is due to the fact that the fault current in inverter dominated grid is limited to 1.2 to 2 times the pre-fault current. During fault F-1 the discrepant impedances estimated for the healthy feeders are shown in Fig. 7. It is seen in Fig. 7, those discrepant impedances are in the vicinity of the origin and with the maximum value of 0.3 Ω which is only about 1% of the line impedances.

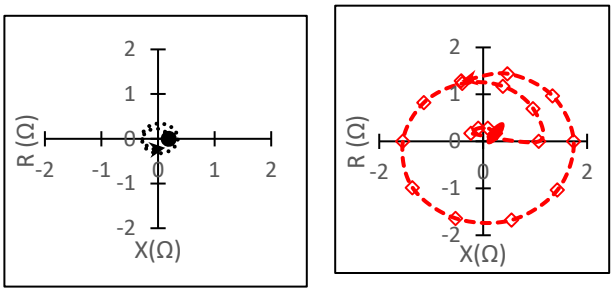

(a) (b)

Fig. 6. Discrepant impedances for feeder between bus-4 and bus- 5 (a) before the fault F1 and (b) during the fault at F-1(1-Φfault at 30% of line length).

The values of discrepant impedances are not exactly at the origin due to the effect of fault F-1 on the rest of the network. Since the microgrid is operating in islanded mode, with all inverter-based resources, a fault in any part of the network affects the voltages and currents in other parts of the network because of low short circuit capacity and zero inertia. Despite this, the proposed relay scheme is able to operate properly without any maloperation.

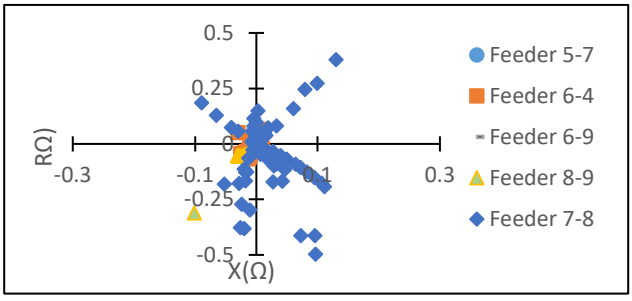

Fig. 7. Discrepant impedances for healthy feeders during a fault at F-1.

When a LL fault, F-2, is simulated at 60 % of the line length from bus 4 on feeder between buses 4 and 5, the estimated discrepant impedances for feeder 4-5 are depicted in Fig. 8 clearly indicating a fault.

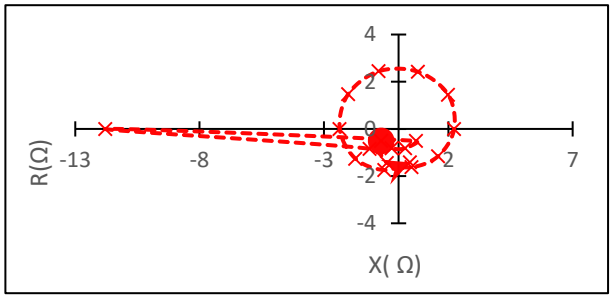

Fig. 8. Discrepant Impedances during a fault F-2 (L-L fault at 60 % of line length) on feeder 4-5.

The discrepant impedances for the rest of the system are shown in Fig. 9 and their values are in the no-fault region.

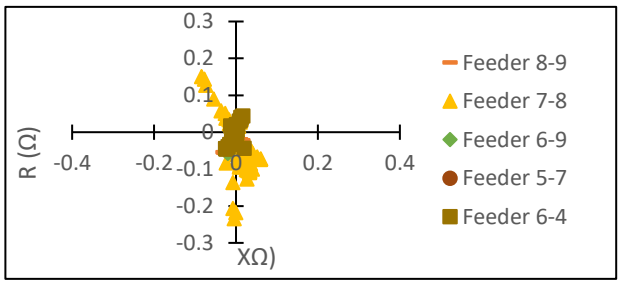

Fig. 9. Discrepant impedances for healthy feeders during a fault at F-2.

Three phase faults are severe faults in a power network. A three-phase fault, F-3, is simulated near bus-5. The discrepant impedances are shown in Fig. 10 and the discrepant impedances of healthy feeders are shown in Fig. 11. The discrepant impedances are in the fault region for the faulty feeder and are in the no-fault region for the healthy feeders.

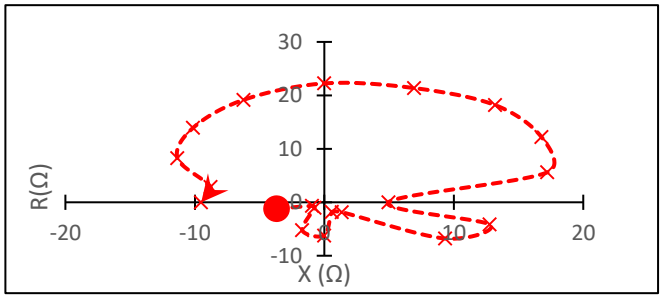

Fig. 10. Discrepant impedances during a fault at F-3(3-Φfault) on feeder 4-5.

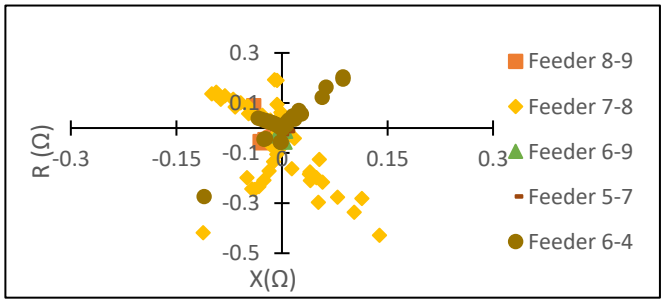

Fig. 11. Discrepant impedances for healthy feeders during a fault at F-3(3-Φ fault).

2) High resistance fault

To verify the performance of the proposed protection scheme during high resistance faults, a L-G fault at F-1 is simulated with a fault resistance of 6 Ω (about 200 % of the feeder impedance). It can be observed from Fig. 12 that the discrepant impedances are in the fault region indicating a fault. The discrepant impedances for healthy feeders during this fault

are in the no-fault region; all of them have small values indicating a no-fault condition.

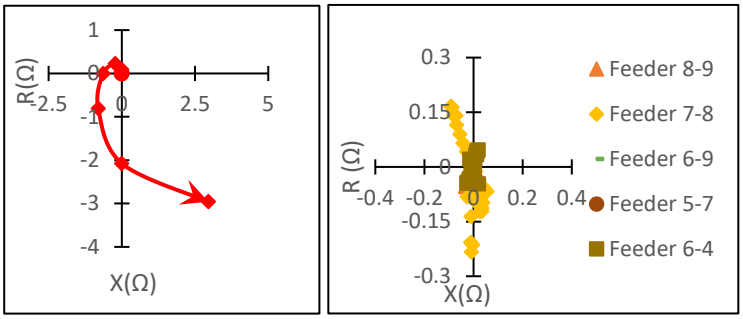

(a) (b)

Fig. 12. (a) Discrepant impedances for feeder between bus-4 and bus- 5 during a high-resistance a fault at F-1 and (b) discrepant impedances of the healthy feeder.

B. *Grid Connected Mode of Operation*

In grid connected mode, when a single-phase fault occurs at F-2 on feeder 4-5, the discrepant impedances estimated by the relay are shown in Fig.13. It is observed that before the fault the impedances are in the no-fault region and during fault, the impedances are in the fault region, while discrepant impedances for the rest of the feeders are in the no-fault region.

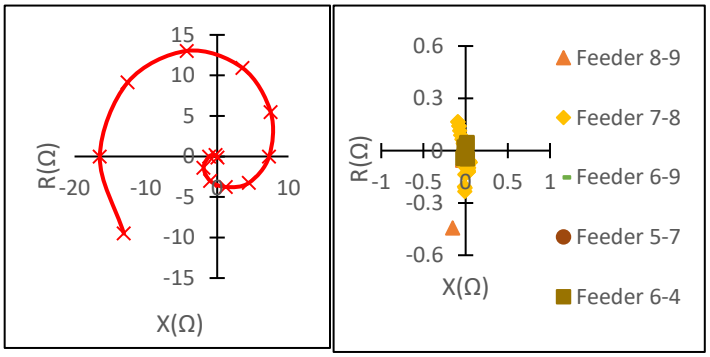

(a) (b)

Fig. 13. (a) Discrepant impedances for feeder between bus-4 and bus- 5 during a high-resistance a fault at F-2 and (b) discrepant impedances of the healthy feeders.

IV. Real Time Implementation

To further verify the proposed protection scheme, a real-time test platform is developed as represented in Fig. 14. The real time implementation is carried out to verify the impact on relays of the healthy feeder when the breakers of the faulty feeder clear the fault. The real time system comprises of GPC rack, GTWIF and GTNeT cards which are used for relay implementation while Novacor® which consists of GNETx2 is used for power system network modeling. Novacor® and GPC rack is connected through a global bus hub (GBH) cable and fiber optic (FO) cables. The samples of voltages and currents are exchanged through GTNeT on sampled values protocol at a rate of 960 HZ.

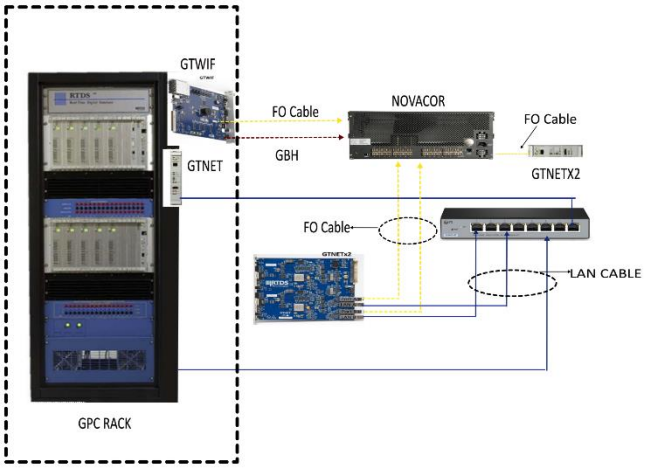

Fig. 14. A real time test platform.

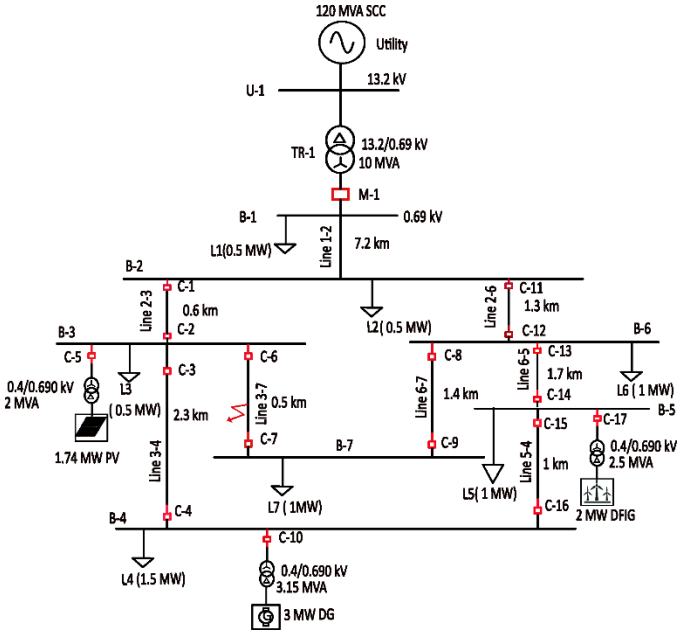

Fig. 15. Single line diagram of a medium voltage microgrid modeled for real time testing.

A. *Real-Time Experiment Results*

A medium voltage microgrid [29], shown in Fig. 15, is modeled in RSCAD to demonstrate and evaluate the proposed protection scheme. The microgrid consists of a 2 MW wind turbine generator,1.7 MW PV generator, and 3 MW diesel generator. All the generation sources are interfaced with the network through a 0.69/13.2 kV transformer. Line parameters of feeders are given in Table-III of Appendix. The microgrid is operated in grid connected mode as well as in islanded mode by operating beaker M-1.

1) Grid Connected mode of operation

Multiple cases have been simulated in grid connected mode of operation of a microgrid. The samples of voltages and currents of bus B-3 and B-7 are provided to the relay. The discrepant impedances are computed by the relay.

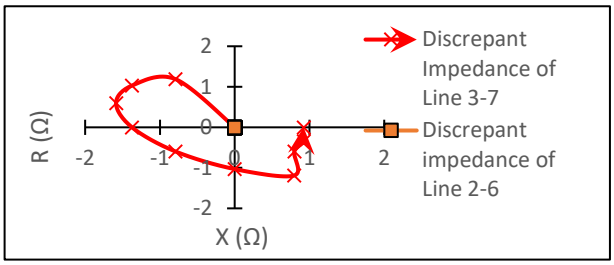

Fig. 16. Discrepant impedances of line 3-7 and line 2-6 during LG fault (Grid connected mode).

It can be observed from Fig. 16 that discrepant impedances for line 3-7 before the fault are in the no-fault region and once the fault occurs, the values are in the fault region. The relay computes discrepant impedances continuously. Once fault strikes on the feeder 3-7, the discrepant impedances are in the fault region and the relay issues a trip signal to the breaker after 1/4 cycle and once the relay issues a trip, the breaker clears the fault in 6 cycles as shown in Fig. 17. However, as seen in Fig. 16, the discrepant impedances of adjacent healthy line 2-6 is not affected and are in the no-fault region before the fault and after fault clearance.

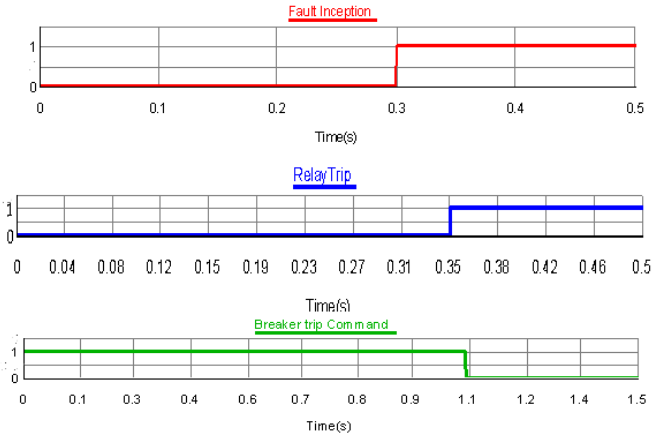

Fig. 17. Timing diagram depicting fault occurrence, relay operation and breaker tripping.

2) Islanded mode of operation

It can be observed from Fig. 18 that the discrepant impedances for line 3-7 computed during the fault are in the fault region, while discrepant impedance on the healthy feeder 2-6 are in the no-fault region before, during and after the fault is cleared.

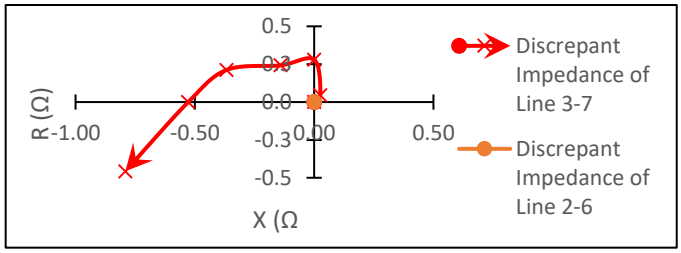

Fig. 18. Discrepant impedances of line 3-7 and line 2-6 for a line-to-line to ground fault

V. Comparison with Differential Protection

In industry, two types of differential protection are commonly used a) current differential using an alpha plane characteristic [30] and b) percentage differential relay. As demonstrated in this section, both differential protection methods do not protect a microgrid in the islanded mode of operation. On the other hand, the protection technique proposed in this paper works properly in both islanded and grid connected modes. To verify this problem associated with line differential relay with an alpha plane characteristic, a L-L fault at F-2 is simulated on a test microgrid shown in Fig. 4, and the response of the relay is shown in Fig 19.

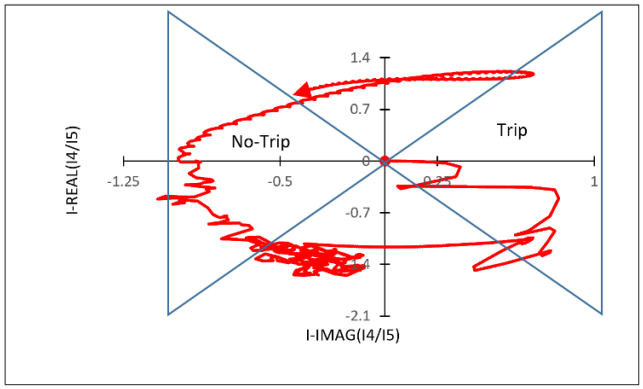

Fig. 19. Differential relay (alpha plane) response for fault F-2 in Fig. 4.

The trajectory of the operating quantity doesn't go into the trip zone, therefore relay does not operate for this fault. As shown in Fig.8. discrepant impedances for the same fault fall in the fault region and the proposed relay will trip. To demonstrate the problem with the percentage differential relay, a LG fault is simulated on line 3-7 of a microgrid shown in Fig. 15 when DG capacity is 2 MW and load L-6 is removed.

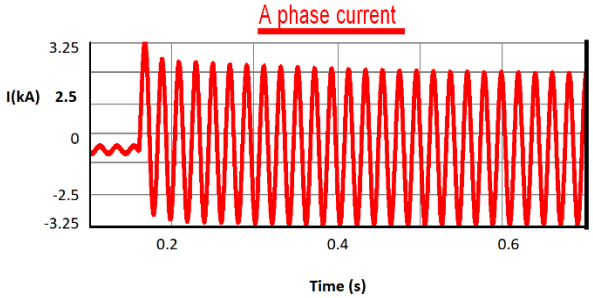

Fig. 20. Current for a L-G fault on line 3-7 during grid-connected mode.

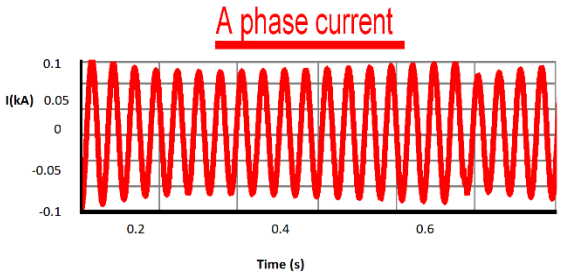

Fig. 21. Current for a L-G fault on line 3-7 during islanded mode.

During grid-connected mode, the fault current is I_{max}= 2.33 kA and during islanded mode, it is I_{min}=0.1 kA which can be observed from Fig. 20 and Fig. 21 respectively. The setting of the differential relay is chosen to be 0.065 times the maximum fault current [31]. Therefore, the differential relay is set at, 0.065 *x* 2.33 kA which is 0.151 kA. The set value is higher than the minimum fault current observed when the microgrid is in the islanded mode of operation. Therefore, the differential will not operate in islanded mode due to the dynamic nature of the fault current. The discrepant impedances in islanded mode and grid connected modes are shown Fig. 22(a) and 22(b) respectively. The discrepant impedances in both cases are in the fault region indicating correct operation of the proposed relaying scheme.

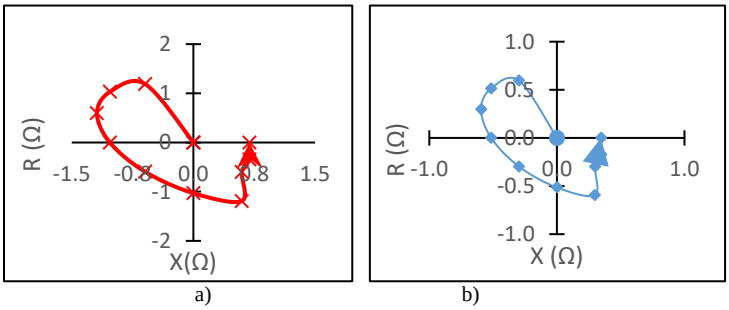

Fig. 22. Discrepant Impedances for a L-G fault on line 3-7 during a) Islanded mode and b) grid connected mode.

VI. Practical Implementation

The proposed protection scheme can be realized either as a centralized protection scheme or as a decentralized protection scheme as depicted in Fig. 23. In centralized protection scheme, the data from PMUs located at the ends of the line are transferred to a central unit where protection algorithm is implemented for all lines in the microgrid. In small microgrids, PMUs can be replaced with merging units, voltage and current samples can be transferred via IEC 61850 protocol to the central unit. In decentralized protection scheme the voltage and current samples are exchanged between relays and each relay implements the proposed relay algorithm and scheme. A hybrid architecture of centralized and decentralized can also be impleted provided that relays are intellegient with features of phasor measurement and handling IEC 61850-9-2 sampled value communication. The medium used for data exchange bewteen relays, PMUs and merging units can be wired or wireless depending on the geographical location of the microgrid.

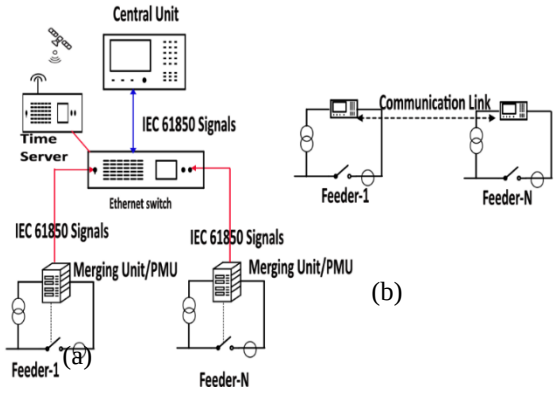

Fig. 23. (a) Centralized protection scheme (b) Decentralized protection scheme.

VII. Conclusions

This paper presents a new microgrid feeder protection technique that uses positive sequence voltages and currents from both ends of the feeder. The technique estimates the discrepant impedance of the feeder under protection. The proposed protection scheme has been tested using PSCAD simulations as well as via real-time implementation. Results demonstrated the effectiveness of the technique in detecting and clearing faults in a variety of situations i.e. islanded mode, grid-connected mode and for various faults including high-resistance faults. The results prove that the proposed protection scheme is effective irrespective of the type of inverter, microgrid topology, inverter control philosophy, level of inverter-based generation and mode of operation. The proposed scheme is fast to detect all types of faults in less than ½ cycle. The technique can be implemented as a centralized, decentralized protection scheme or as a hybrid protection scheme.

VIII. Appendix : Test System Data

Table. I
Load and Generation Values of the Test System in Figure 4

Bus	Bus Voltage (kV)	Inverter/ Load	P (MW)	Q (MVAR)
Bus-1	16.5	GFM	66.9	16.1
Bus-2	18	GFL	163.6	5.0
Bus-3	13.8	GFM	89.9	-5
Bus-5	230	Fixed load	125	5
Bus-6	230	Fixed load	90	3
Bus-8	230	Fixed load	100	3

Table. II
Line Parameters of the Test System in Figure 4

Sequence	R (ohm/m)	XL((ohm/m)	XC(ohm/m)
Positive	1.07×10^{-4}	4.27×10^{-4}	2.5448×10^{6}
Zero	5.35×10^{-4}	1.153×10^{-3}	4.1642×10^{6}

Note: Line length between any two bus is 10 km.

TABLE. III
LINE PARAMETERS OF THE TEST SYSTEM IN FIGURE 15

Sequence	R (ohm/m)	XL((ohm/m)	XC(ohm/m)
Positive	1.73×10^{-4}	4.317×10^{-4}	3.626×10^{6}
Zero	3.5×10^{-4}	1.79×10^{-3}	8.846×10^{6}

REFERENCES

[1] S. Parhizi, H. Lotfi, A. Khodaei, and S. Bahramirad, "State of the Art in Research on Microgrids: A Review," *IEEE Access*, vol. 3, pp. 890–925, 2015, doi: 10.1109/ACCESS.2015.2443119.

[2] Pan Nianan and Wang Luyang, *PSCAD Studies Demonstrate Grid Forming Inverters Can Improve Weak Grid of Australia*. [Online]. Available:https://en.sungrowpower.com/upload/file/20211201/Grid%20Forming%20Whitepaper.pdf

[3] R. W. Kenyon, A. Sajadi, A. Hoke, and B.-M. Hodge, "Open-Source PSCAD Grid-Following and Grid-Forming Inverters and A Benchmark for Zero-Inertia Power System Simulations," in *2021 IEEE Kansas Power and Energy Conference (KPEC)*, Manhattan, KS, USA, Apr. 2021, pp. 1–6. doi: 10.1109/KPEC51835.2021.9446243.

[4] A. Srivastava, R. Mohanty, M. A. F. Ghazvini, L. A. Tuan, D. Steen, and O. Carlson, "A Review on Challenges and Solutions in Microgrid Protection," in *2021 IEEE Madrid PowerTech*, Madrid, Spain, Jun. 2021, pp. 1–6. doi: 10.1109/PowerTech46648.2021.9495090.

[5] S. S. Rath, G. Panda, P. K. Ray, and A. Mohanty, "A Comprehensive Review on Microgrid Protection: Issues and Challenges," in *2020 3rd International Conference on Energy, Power and Environment: Towards Clean Energy Technologies*, Shillong, Meghalaya, India, Mar. 2021, pp. 1–6. doi: 10.1109/ICEPE50861.2021.9404520.

[6] M. W. Altaf, M. T. Arif, S. Saha, S. N. Islam, M. E. Haque, and Amt. Oo, "Renewable Energy Integration challenge on Power System Protection and its Mitigation for Reliable Operation," in *IECON 2020 The 46th Annual Conference of the IEEE Industrial Electronics Society*, Singapore, Oct. 2020, pp. 1917–1922. doi: 10.1109/IECON43393.2020.9254380.

[7] Central Power Research Institute *et al.*, "Protection challenges under bulk penetration of renewable energy resources in power systems: A review," *CSEE JPES*, vol. 3, no. 4, pp. 365–379, Dec. 2017, doi: 10.17775/CSEEJPES.2017.00030.

[8] J. Shiles *et al.*, "Microgrid protection: An overview of protection strategies in North American microgrid projects," in *2017 IEEE Power and Energy Society General Meeting*, Chicago, IL, Jul. 2017, pp. 1–5. doi: 10.1109/PESGM.2017.8274519.

[9] M. N. Alam, S. Chakrabarti, and A. K. Pradhan, "Protection of Networked Microgrids Using Relays With Multiple Setting Groups," *IEEE Trans. Ind. Inf.*, vol. 18, no. 6, pp. 3713–3723, Jun. 2022, doi: 10.1109/TII.2021.3120151.

[10] T. S. Sidhu and D. Bejmert, "Short-circuit current contribution from large scale PV power plant in the context of distribution power system protection performance," in *IET Conference on Renewable Power Generation (RPG 2011)*, Edinburgh, UK, 2011, pp. 134–134. doi: 10.1049/cp.2011.0153.

[11] T. Neumann and I. Erlich, "Short Circuit Current Contribution of a Photovoltaic Power Plant," *IFAC Proceedings Volumes*, vol. 45, no. 21, pp. 343–348, 2012, doi: 10.3182/20120902-4-FR-2032.00061.

[12] J. Li, X. Zhang, W. Yao, J. Xu, X. Shi, and F. Ren, "Inverse Time Differential Current Protection for Microgrid," in *2022 IEEE 5th International Electrical and Energy Conference (CIEEC)*, Nangjing, China, May 2022, pp. 590–595. doi: 10.1109/CIEEC54735.2022.9845849.

[13] Power System Relaying and Control CommitteeWorking Group C30, "Microgrid protection System," IEEE, Technical report PES-TR71, Jul. 2019. [Online]. Available: https://resourcecenter.ieee-pes.org/publications/technical-reports/PES_TP_TR71_PSRC_microgrid_082019.html

[14] Z. Shuai, C. Shen, X. Yin, X. Liu, and Z. J. Shen, "Fault Analysis of Inverter-Interfaced Distributed Generators With Different Control Schemes," *IEEE Trans. Power Delivery*, vol. 33, no. 3, pp. 1223–1235, Jun. 2018, doi: 10.1109/TPWRD.2017.2717388.

[15] E. Sortomme, J. Ren, and S. S. Venkata, "A differential zone protection scheme for microgrids," in *2013 IEEE Power and Energy Society General Meeting*, Vancouver, BC, 2013, pp. 1–5. doi: 10.1109/PESMG.2013.6672113.

[16] T. S. Ustun, C. Ozansoy, and A. Zayegh, "Differential protection of microgrids with central protection unit support," in *IEEE 2013 Tencon - Spring*, Sydney, Australia, Apr. 2013, pp. 15–19. doi: 10.1109/TENCONSpring.2013.6584408.

[17] E. Casagrande, W. L. Woon, H. H. Zeineldin, and D. Svetinovic, "A Differential Sequence Component Protection Scheme for Microgrids With Inverter-Based Distributed Generators," *IEEE Trans. Smart Grid*, vol. 5, no. 1, pp. 29–37, Jan. 2014, doi: 10.1109/TSG.2013.2251017.

[18] R. Lasseter and H. Nikkhajoei, "Microgrid Protection," p. 6.

[19] B. Liao, J. Cheng, and G. Ren, "Microgrid Adaptive Current Instantaneous Trip Protection," in *2019 IEEE Innovative Smart Grid Technologies - Asia (ISGT Asia)*, Chengdu, China, May 2019, pp. 2074–2078. doi: 10.1109/ISGT-Asia.2019.8881166.

[20] T. Patel, S. Brahma, J. Hernandez-Alvidrez, and M. J. Reno, "Adaptive Protection Scheme for a Real-World Microgrid with 100% Inverter-Based Resources," in *2020 IEEE Kansas Power and Energy Conference (KPEC)*, Manhattan, KS, USA, Jul. 2020, pp. 1–6. doi: 10.1109/KPEC47870.2020.9167527.

[21] T. E. Sati and M. A. Azzouz, "Optimal Protection Coordination for Inverter Dominated Islanded Microgrids Considering N-1 Contingency," *IEEE Trans. Power Delivery*, vol. 37, no. 3, pp. 2256–2267, Jun. 2022, doi: 10.1109/TPWRD.2021.3108760.

[22] S. Gopalan, V. Sreeram, H. Iu, and Y. Mishra, "An improved protection strategy for microgrids," in *IEEE PES ISGT Europe 2013*, Lyngby, Denmark, Oct. 2013, pp. 1–5. doi: 10.1109/ISGTEurope.2013.6695477.

[23] M. A. Haj-ahmed and M. S. Illindala, "The Influence of Inverter-Based DGs and Their Controllers on Distribution Network Protection," *IEEE Trans. on Ind. Applicat.*, vol. 50, no. 4, pp. 2928–2937, Jul. 2014, doi: 10.1109/TIA.2013.2297452.

[24] C. A. Plet, M. Graovac, T. C. Green, and R. Iravani, "Fault response of grid-connected inverter dominated networks," in *IEEE PES General Meeting*, Minneapolis, MN, Jul. 2010, pp. 1–8. doi: 10.1109/PES.2010.5589981.the

[25] M. J. Reno, S. Brahma, A. Bidram, and M. E. Ropp, "Influence of Inverter-Based Resources on Microgrid Protection: Part 1: Microgrids in Radial Distribution Systems," *IEEE Power and Energy Mag.*, vol. 19, no. 3, pp. 36–46, May 2021, doi: 10.1109/MPE.2021.3057951.

[26] A. Hooshyar and R. Iravani, "A New Directional Element for Microgrid Protection," *IEEE Trans. Smart Grid*, vol. 9, no. 6, pp. 6862–6876, Nov. 2018, doi: 10.1109/TSG.2017.2727400

[27] Behnam Mahamedi, John Edward Fletcher, "Trends in the protection of inverter-based Microgrids", IET Gener. Transm. Distrib., 2019, Vol. 13 Iss. 20, pp. 4511-4522.

[28] "A Protection Method for Inverter-based Microgrid Using Current-only Polarity Comparison," in Journal of Modern Power Systems and Clean Energy, vol. 8, no. 3, pp. 446-453, May 2020, doi: 10.35833/MPCE.2018.000722.

[29] O. Nzimako and A. Rajapakse, "Real time simulation of a microgrid with multiple distributed energy resources," 2016 International Conference on Cogeneration, Small Power Plants and District Energy (ICUE), Bangkok, Thailand, 2016, pp. 1-6, doi: 10.1109/COGEN.2016.7728945.

[30] G. Benmouyal, "The Trajectories of Line Current Differential Faults in the Alpha Plane," Line Current Differential Protection: A Collection of Technical Papers Representing Modern Solutions, 2014, Schweitzer Engineering Laboratories, Inc.

[31] Shi Chen et al, " Sequence-component-based current differential protection for transmission lines connected with IIGs", IET Gener. Transm. Distrib., 2018, Vol. 12 Iss. 12, pp. 3086-3096.